

Journal of Materials Chemistry A

Accepted Manuscript



This is an *Accepted Manuscript*, which has been through the Royal Society of Chemistry peer review process and has been accepted for publication.

Accepted Manuscripts are published online shortly after acceptance, before technical editing, formatting and proof reading. Using this free service, authors can make their results available to the community, in citable form, before we publish the edited article. We will replace this *Accepted Manuscript* with the edited and formatted *Advance Article* as soon as it is available.

You can find more information about *Accepted Manuscripts* in the [Information for Authors](#).

Please note that technical editing may introduce minor changes to the text and/or graphics, which may alter content. The journal's standard [Terms & Conditions](#) and the [Ethical guidelines](#) still apply. In no event shall the Royal Society of Chemistry be held responsible for any errors or omissions in this *Accepted Manuscript* or any consequences arising from the use of any information it contains.

Cite this: DOI: 10.1039/c0xx00000x

www.rsc.org/xxxxxx

ARTICLE TYPE

Hybridization of brookite TiO₂ with *g*-C₃N₄: A visible-light-driven photocatalyst for As³⁺ oxidation, MO degradation and water splitting for hydrogen evolution

Yipeng Zang,^{a,b} Liping Li,^a Yangsen Xu,^a Ying Zuo,^a and Guangshe Li^{*a}⁵ Received (in XXX, XXX) Xth XXXXXXXXX 20XX, Accepted Xth XXXXXXXXX 20XX

DOI: 10.1039/b000000x

This work gives a first report on the effective visible-light-driven photocatalyst of brookite TiO₂ (br-TiO₂) hybridized with *g*-C₃N₄. This hybrid was prepared via a facile calcination in air. When irradiated under visible light, all br-TiO₂/*g*-C₃N₄ hybrids showed an activity superior to the component *g*-C₃N₄ or br-TiO₂ in MO degradation. The optimum photocatalytic activity of the hybrid br-TiO₂/*g*-C₃N₄ is higher than those of other types of TiO₂ (anatase and rutile) when hybridized with *g*-C₃N₄. Furthermore, the optimized hybrid, br-TiO₂/*g*-C₃N₄ (35 wt%) was successfully applied to toxic As³⁺ oxidation and water splitting for hydrogen generation under visible light. All these results clearly demonstrate that the hybridization of br-TiO₂ with *g*-C₃N₄ is highly promising for photocatalytic uses, which are barely accessible in previous literature. This abnormal observation is ascribed to the effective separation of the photo-generated carriers on the surfaces between the closely contacted br-TiO₂ and *g*-C₃N₄.

1. Introduction

Energy and environment issues could be effectively solved by technology based on photocatalysis for its strong ability in pollutant degradation, hydrogen generation and greenhouse gas reduction.¹⁻⁹ TiO₂ is a popular photocatalyst, which contains three different crystal phases: anatase, rutile and brookite (br-TiO₂).¹⁰⁻¹² Among all these phases, both anatase and rutile are widely studied for improved photocatalytic performance.¹³⁻¹⁵ Alternatively, br-TiO₂ is usually regarded as an inert photocatalyst,¹⁶ and its difficult synthesis limits further studies. Through a spatial charge transfer control with specific surface exposure, our group has recently made a progress in tuning br-TiO₂ from inert to highly reactive towards MO degradation, which even shows a catalytic performance superior to P25.¹⁷ Nevertheless, the relevant results are still not wholly satisfactory, since just like other types of TiO₂ family, br-TiO₂ can only work under ultraviolet-light irradiation due to its wide band gap. As a consequence, it is very interesting, but highly challenging to find br-TiO₂-based photocatalysts that can work under visible light for multi-photocatalytic applications.

We propose that if wide-band gap br-TiO₂ could combine with proper narrow-band gap semiconductors to form a hybrid, it is most likely to work under visible-light irradiation and to efficiently separate the photo-generated carriers for excellent activity. The relevant narrow-band gap semiconductors have to meet two requirements: (i) the band gap should be narrow enough so as to absorb visible-light, and (ii) the band position should match that of br-TiO₂. In this regard, graphite carbon nitride (*g*-C₃N₄) could be suitable to hybridize with br-TiO₂, since it is a typical metal-free polymer semiconductor with a narrow band gap of 2.7 eV. There have been many studies on hybrids of *g*-C₃N₄ with other forms of TiO₂.¹⁸⁻²² Recent studies on this π -

conjugated photocatalyst have shown certain photocatalytic activity in MO degradation and hydrogen production under visible-light irradiation.^{23,24} On the other hand, the band position of *g*-C₃N₄ matches well that of br-TiO₂, which is beneficial for the separation of photo-generated carriers on the interfaces between br-TiO₂ and *g*-C₃N₄. So, if a hybrid could be prepared between br-TiO₂ and *g*-C₃N₄, one may expect to create a new multi-purpose photocatalyst driven by visible-light.

In this work, we chose MO degradation, As³⁺ oxidation and hydrogen production from water as the model catalytic reactions. Hybrid br-TiO₂/*g*-C₃N₄ was first synthesized by a facile calcination. It is found that the hybrid exhibited an excellent photocatalytic activity towards MO degradation and As³⁺ oxidation under visible-light irradiation, which is much higher than those of the component br-TiO₂ or *g*-C₃N₄. When involving traces of Pt additives, the hybrid was well used for hydrogen evolution from water. The findings reported here have not even been accessible in the previous literature for a single photocatalyst to have multi-catalytic uses under visible-light irradiation.

2. Experimental

2.1 Catalyst Synthesis

All chemicals were purchased from Sinopharm Chemical Reagent Corp and used without further purification.

Synthesis of g-C₃N₄: 5 g melamine was heated in a semi-closed crucible at 520 °C for 4 h, and the heating rate was set at 20 °C/min.

*Synthesis of br-TiO₂/*g*-C₃N₄ composite*: Pure brookite TiO₂ was prepared as our previous report.¹⁷ The resulted TiO₂ nanocrystals were named as TiO₂-O. After ultrasonication for 30 min, TiO₂-O was added into the *g*-C₃N₄ and ethanol mixture, and the slurry was put in a fume hood and stirred for 24 h. These dried products

were calcined at 400 °C for 1 h. For comparison, sample TiO₂-O was also annealed at 400 °C for 1 h and named as br-TiO₂. The hybrid br-TiO₂/g-C₃N₄ samples were named as br-TiO₂/g-C₃N₄-x%, where x% is the weight ratio of the g-C₃N₄.

2.2 Sample Characterization

Rigaku MinFlexII benchtop X-ray diffractometry (XRD) with Cu-Kα irradiation was applied to investigate the crystal structures of the samples. A monochromatic Al Kα X-ray source with 150 W was taken for the characterization of X-ray photoelectron spectroscopy (XPS). The morphology for the as-obtained samples was characterized by transmission electron microscope (TEM, Tecnai G2 F20). Varian Cary-500 spectrophotometer was used to measure the UV-vis diffuse reflection spectroscopy (DRS) of the samples. Nitrogen absorption data were used to measure the specific surface area of these samples at liquid nitrogen temperature on a Micromeritics Tristar 3000. Photoluminescence (PL) spectra of the samples were recorded using a Varian Cary Eclipse Fluorescence Spectrometer at room temperature. A three-electrode system was taken for Electrochemical impedance spectroscopy (EIS) measurements (CHI 660E, Shanghai, China), in which reference electrode was Ag/AgCl, the counter electrode platinum sheet, and indium-tin oxide (ITO) glass as the working electrode. The working electrode was modified in this way: 0.5 mL DMF was chosen as solvent, 5 mg g-C₃N₄ and br-TiO₂/g-C₃N₄-35% are added to DMF, respectively. After ultrasonication for 30 min, the as-prepared slurry was dripped on 0.5 cm×0.5 cm ITO glass, dried at 60 °C for 4 h. For comparison, the content of the dripped g-C₃N₄ slurry was consistent with br-TiO₂/g-C₃N₄-35%.

2.3 Photocatalytic activity measurements

2.3.1 MO degradation

Methyl orange (MO) degradation under visible-light irradiation was chosen as a probe reaction to evaluate the photocatalytic activities of these samples. For this experiment, 100 mg samples were added to 100 mL MO aqueous solution (10 ppm) with stirring. Before photocatalytic reaction, the adsorption and desorption balance of the tested catalyst with MO aqueous solution was obtained by magnetically stirred in dark for 5 h. This degradation process was executed at room temperature, the pH value of the solution was adjusted as 7, and the stirring is accompanied with the reaction. A 300 W Xe lamp was applied as light source which was equipped with a UV-cutoff filter (>420 nm) to remove the UV-light. The irradiated solution was taken every 30 minutes.

2.3.2 As³⁺ oxidation

We also employed As³⁺ removal experiments to characterize the photocatalytic activity of the as-synthesized samples. In the As³⁺ removal experiments, 5 ppm NaAsO₂ solution was used as probe substrate. 80 mg photocatalysts were dispersed in the NaAsO₂ solution with stirring, and the pH of the solution was adjusted to 7 by 1 mol/L NaOH. Before the light irradiation, this mixture was magnetically stirred in dark for 5 h to establish an adsorption and desorption balance. A 300 W Xe lamp equipped with a 420 nm

and 300 nm cutoff filter was employed to obtain the visible-light and UV-light, respectively. The content of As³⁺ in the reaction solution was detected by Atomic Fluorescence Spectrometry (PF6, Beijing, China).

2.3.3 Hydrogen generation

Hydrogen production performance of these samples was studied using a 150 mL Pyrex flask reactor. The light source is given by a 300 W Xe lamp equipped with a UV-cutoff filter (>400 nm) to obtain visible-light. In the photocatalytic process, 50 mg samples and 45 mL deionized water were added into the flask. 5 mL triethanolamine which acted as sacrificial agent were added. H₂PtCl₆ solution (1.0 wt% for Pt) acts as co-catalyst to improve the photocatalytic performance of these samples was used. It is worth noting that the residual air of the photocatalytic reactor was deprived by vacuum pump and kept sealed during the visible light irradiation. The time of experiment was set at 3 hours, and gas chromatograph (Fuli 9790 II, Zhejiang, China) with TCD detector was carried to detect the photo-generated gas in every 1 h.

3. Results and Discussion

3.1 Preparation of br-TiO₂/g-C₃N₄ hybrids

XRD technique was used to identify the phase compositions of the samples. Fig. 1 shows the XRD patterns of these hybrids, br-TiO₂/g-C₃N₄ and the components g-C₃N₄ and br-TiO₂. It is clearly seen in Fig. 1 that when varied with different contents of g-C₃N₄, all diffraction peaks of the samples could be well divided into two sets of data for g-C₃N₄ and br-TiO₂. The component g-C₃N₄ is characterized by two diffraction signals at two theta of 13.2 and 27.4 degrees, which are corresponding to inter-layer structural packing and stacking of the conjugated aromatic system, respectively.²⁵ For another component of br-TiO₂, the relevant diffraction peaks are well assigned to the brookite phase (JCPDS, No. 29-1360). With increasing the content of g-C₃N₄, the diffraction peak at two theta of 27.4 degree becomes strong.

FT-IR spectroscopy is applied to study the compositions of the samples, as displayed in Fig. S1. For hybrid br-TiO₂/g-C₃N₄, all IR data were consisted of two sets of characteristic absorptions: one set corresponds to g-C₃N₄ that contains the absorptions at wave-numbers of 808, 1242, 1320 to 1633 cm⁻¹. The triazine units of g-C₃N₄ are reflected by the absorption at 808 cm⁻¹. The stretching vibration of C-N heterocyclics is indicated by the absorptions in the region from 1242 to 1574 cm⁻¹. The absorptions at 1321 and 1633 cm⁻¹ indicate the presence of C-N and C=N stretching mode, respectively.^{26,27} Another set is ascribed to br-TiO₂, as indicated by the absorptions at 422 and 526 cm⁻¹. All these data demonstrate that the hybrid br-TiO₂/g-C₃N₄ contains g-C₃N₄ and br-TiO₂, which are consistent with our XRD data analysis.

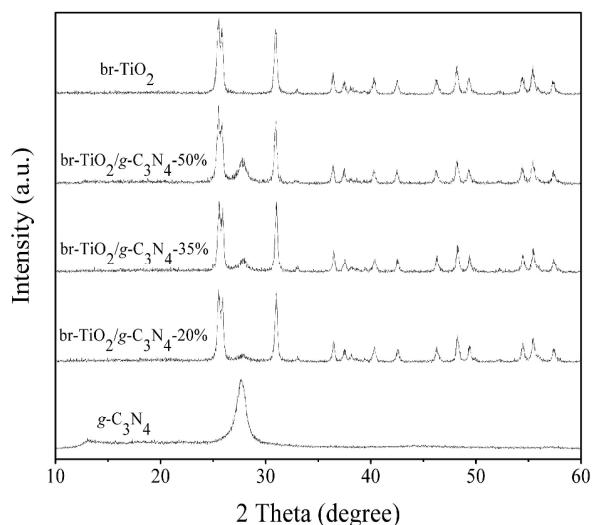


Fig. 1 XRD patterns of the hybrid br-TiO₂/g-C₃N₄ with different contents of g-C₃N₄. For comparison, pure br-TiO₂ and g-C₃N₄ were also given.

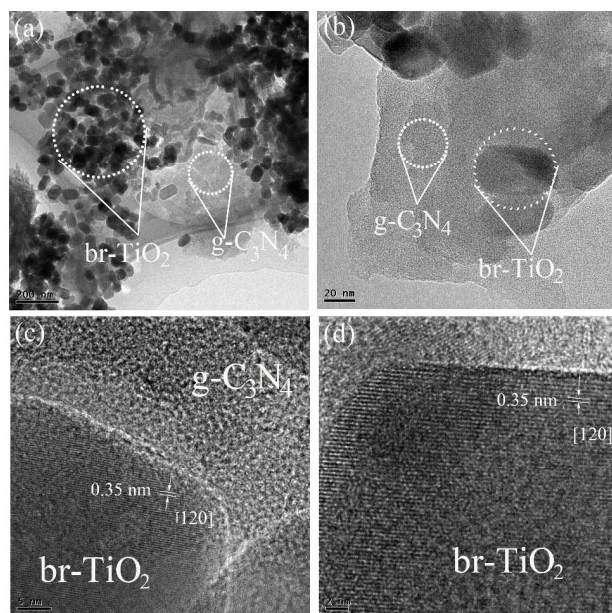


Fig. 2 (a, b) TEM and (c, d) HRTEM images for the as-prepared br-TiO₂/g-C₃N₄ hybrid.

The hybridization between brookite TiO₂ and g-C₃N₄ was further confirmed by high resolution TEM, as shown in Fig. 2. It can be found from Fig. 2(a-b) that component g-C₃N₄ showed a sheet shape, while the component br-TiO₂ appeared in nanoparticles with an average diameter of approximately 40 nm, which are dispersed well on the surface of g-C₃N₄. As indicated by HRTEM images in Fig. 2(c-d), spacing of 0.35 nm is corresponding to the crystalline faces [120] of br-TiO₂. Importantly, the close contact between br-TiO₂ and g-C₃N₄ in Fig. 2c illustrated that the annealing process is necessary for those integrated composites and further for superior catalytic performance.

The electronic states of the elements for the as-prepared hybrids were further studied by XPS. Fig. S2 gives the survey scan results of br-TiO₂/g-C₃N₄-35% and br-TiO₂. The measurement result reveals the presence of Ti, O, C, and N for

the hybrid.

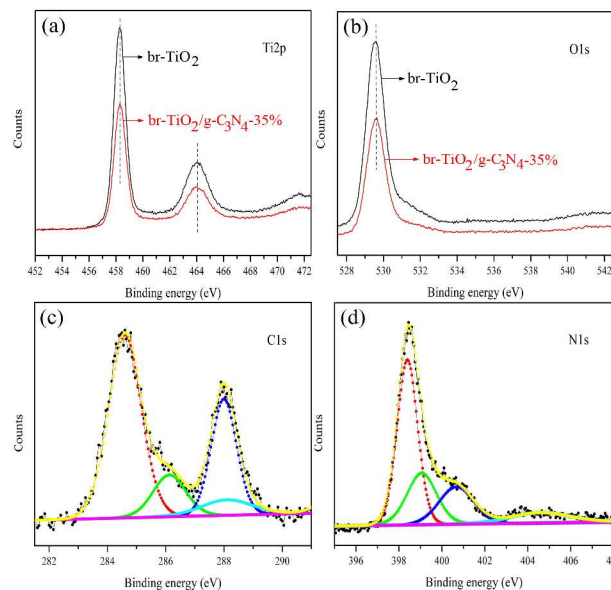


Fig. 3 High resolution XPS scan of the as-prepared hybrid br-TiO₂/g-C₃N₄ and br-TiO₂: (a) Ti2p; (b) O1s; (c) C1s; and (d) N1s.

High resolution XPS spectra of Ti 2p, O 1s, C 1s, and N 1s for the hybrid are shown in Fig. 3. Fig. 3a compares the XPS spectra of Ti 2p for br-TiO₂/g-C₃N₄-35% with that of br-TiO₂. Two signals at binding energies of 458.2 and 464.1 eV refer to Ti2p_{3/2} and Ti2p_{1/2}, respectively. As reported in a former literature,²⁸ this value is highly consistent with the binding energy of Ti⁴⁺ ion in br-TiO₂. The characteristic binding energy of O 1s in br-TiO₂ and br-TiO₂/g-C₃N₄ is 529.5 eV with no significant change, as indicated by high resolution XPS spectra in Fig. 3b. Several signals in Fig. 3c with binding energies of 284.6, 286.1, 287.7, and 288.1 eV are ascribed to those for C 1s of br-TiO₂/g-C₃N₄-35%. It is well known that the C1s signal for graphitic carbon appears at 284.6 eV, and the combination of C-N groups shows the C1s signal at 286.1 eV. The signal at binding energy of 287.9 eV comes from C=N coordination. Finally, the signal at 288.1 eV is characteristic of sp² C atoms from N-C=N coordination. Fig. 3d displays the high resolution XPS spectra of N 1s for br-TiO₂/g-C₃N₄-35%. One can see several sub-lines with binding energies at 398.4, 399.1, 400.7, and 404.5 eV that are composed in the spectra. The sp²-hybridized aromatic N bound to C atoms shows the signal at 398.4 eV, while the signal at binding energy of 399.1 eV indicates tertiary N bonded to C atoms in the form of N-(C)₃. The signals at 400.7 and 404.5 eV are assigned to the N-H structure and π excitation, respectively.^{29,30}

Table 1 shows the BET specific surface area of series hybrid br-TiO₂/g-C₃N₄ with different contents of br-TiO₂. For comparison, results of pure g-C₃N₄ and br-TiO₂ are also given. The BET value for br-TiO₂/g-C₃N₄ was 21.3 m²g⁻¹, bigger than that of 16.7 m²g⁻¹ for pure g-C₃N₄ or 16.4 m²g⁻¹ for br-TiO₂. The BET value for the hybrid becomes larger, as the content of g-C₃N₄ increases. The enlargement of the specific surface area about hybrid br-TiO₂/g-C₃N₄ may be closely related to the calcination process as reported in our former report.¹⁸

Table 1. Physicochemical properties of the hybrid br-TiO₂/g-C₃N₄

Samples	<i>g</i> -C ₃ N ₄ content	BET specific surface area (m ² g ⁻¹)	Band gap (eV)
<i>g</i> -C ₃ N ₄	100%	16.7	2.7
br-TiO ₂	0%	16.4	3.2
br-TiO ₂ / <i>g</i> -C ₃ N ₄ -20%	20%	19.4	2.72
br-TiO ₂ / <i>g</i> -C ₃ N ₄ -35%	35%	21.3	2.72
br-TiO ₂ / <i>g</i> -C ₃ N ₄ -50%	50%	23.6	2.72

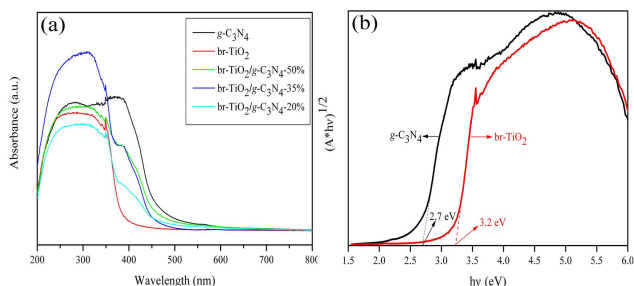


Fig. 4 (a) DRS spectrums of the as-prepared hybrid br-TiO₂/*g*-C₃N₄, br-TiO₂ and *g*-C₃N₄; and (b) Plot of $(h\nu)^{1/2}$ versus energy ($h\nu$) for the band gap energy of br-TiO₂ and *g*-C₃N₄.

DRS analysis was used to study the optical absorption ability of as-prepared hybrid br-TiO₂/*g*-C₃N₄, pure *g*-C₃N₄ and br-TiO₂. For hybrid br-TiO₂/*g*-C₃N₄, the absorption edge moves up at around 456 nm, which compares to that of 463 nm for pure *g*-C₃N₄ or 381 nm for br-TiO₂ (Fig. 4a). These results illustrate that these hybrids br-TiO₂/*g*-C₃N₄ have the ability to absorb visible-light due to the interactions between both components. Further, we applied Eq.(1) to calculate the band gap energies, E_g , of *g*-C₃N₄ and br-TiO₂.

$$\alpha h\nu = k(h\nu - E_g)^{1/n} \quad (1)$$

$$E_g = 1240/\lambda \quad (2)$$

The diagram of calculation is given in Fig. 6b. It should be noted that n in Eq.(1) is determined by the type of optical transition of a semiconductor. Since *g*-C₃N₄ and br-TiO₂ are both indirect semiconductors, the value of n is set at 2, as for other indirect semiconductors¹⁶. On the other hand, Eq.(2) is used to roughly estimate the E_g of hybrid br-TiO₂/*g*-C₃N₄, in which λ refers to the wavelength of absorption edge.³¹ Table 1 gives all estimated results.

3.2 Photocatalytic performance of the br-TiO₂/*g*-C₃N₄ composites

Fig. 5 shows the photocatalytic performance towards MO degradation for the as-prepared samples under visible light. It can be seen that these hybrids br-TiO₂/*g*-C₃N₄ have photocatalytic activity superior to both components of *g*-C₃N₄ and br-TiO₂. For the hybrids br-TiO₂/*g*-C₃N₄ with different contents of *g*-C₃N₄, br-TiO₂/*g*-C₃N₄-35% shows the best activity, as represented by almost 55% decomposition of MO in 180 min. However, only 15% MO is degraded by *g*-C₃N₄, while pure br-TiO₂ shows a negligible activity on MO degradation within the prescribed time. The interactions between components of *g*-C₃N₄ and br-TiO₂ are the consequence of chemical synthesis, which can be the key for the enhanced photocatalytic activity. In order to prove this speculation, we did a parallel experiment, in which the samples were synthesized by physical mixing method, and its photocatalytic activity was evaluated under the same condition.

It reveals that the catalytic performance of the physical mixed sample br-TiO₂/*g*-C₃N₄-PM is compatible with br-TiO₂ but much poorer than *g*-C₃N₄ or hybrid br-TiO₂/*g*-C₃N₄. This result illustrates that the chemically-synthesized samples are superior to the physical mixed sample, which allows us to adjust the content of *g*-C₃N₄ in these hybrids for optimum photocatalytic activity.

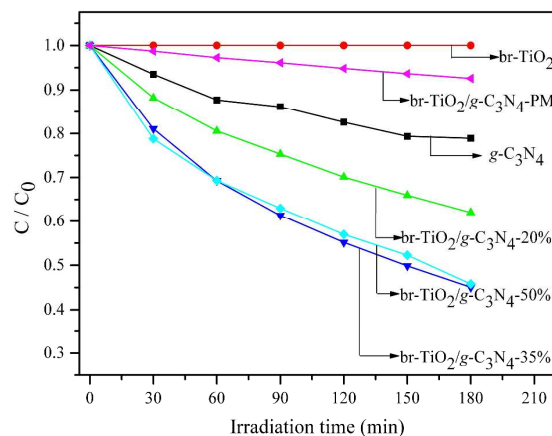


Fig. 5 Photocatalytic activity of the as-prepared hybrid br-TiO₂/*g*-C₃N₄, br-TiO₂ and *g*-C₃N₄ on MO degradation under visible light irradiation.

Reaction kinetic is one of effective methods to evaluate the reaction rate of photocatalytic process. In this case, we employed first-order model to fit the experimental data. Fig. S3 gives the histogram of the rate constant k that changes with the content of *g*-C₃N₄ in these hybrids. It demonstrates that k for br-TiO₂/*g*-C₃N₄-35% of the highest photocatalytic activity is 0.00443 min⁻¹, which is almost 3.4 times larger than that of 0.00131 min⁻¹ for *g*-C₃N₄. Because of the inert activity, k for br-TiO₂ is 0.

The excellent photocatalytic performance of hybrid br-TiO₂/*g*-C₃N₄-35% is further proved by comparing to other composites of crystal phase TiO₂ (anatase and rutile) on MO degradation under visible-light irradiation. As displayed in Fig. S4 for MO photocatalytic efficiency of these samples, the hybrid br-TiO₂/*g*-C₃N₄-35% exhibited the best activity, relative to those of anatase-TiO₂/*g*-C₃N₄-35%, rutile-TiO₂/*g*-C₃N₄-35%, rutile-TiO₂/*g*-C₃N₄-50%. Moreover, the photocatalytic performance of br-TiO₂/*g*-C₃N₄-35%, br-TiO₂ and *g*-C₃N₄ was also studied under UV-light irradiation. As given in Fig. S5, br-TiO₂ also has the best photocatalytic activity on MO degradation.

Hybrid br-TiO₂/*g*-C₃N₄-35% also exhibited an excellent photocatalytic activity towards hydrogen production from water splitting under visible-light irradiation. As indicated in Fig. 6, H₂ evolution rate of br-TiO₂/*g*-C₃N₄-35% is 1058 μmol/gh, much higher than that of 670 μmol/gh for *g*-C₃N₄, when normalized to the weight of *g*-C₃N₄. For br-TiO₂, very little H₂ is produced. So, the hybridization of br-TiO₂ with *g*-C₃N₄ has promoted the photocatalytic performance of *g*-C₃N₄.

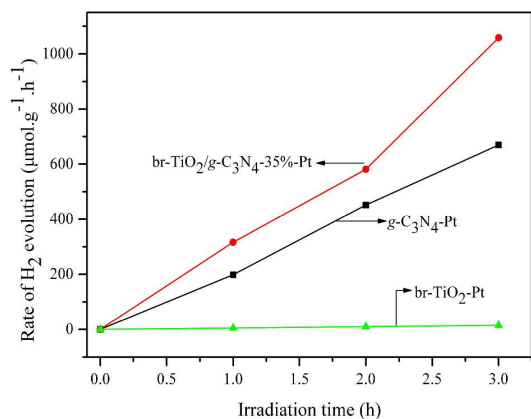


Fig. 6 Comparison of hydrogen generation rate of the hybrid br-TiO₂/g-C₃N₄-35% with those of br-TiO₂ and g-C₃N₄ under visible light irradiation.

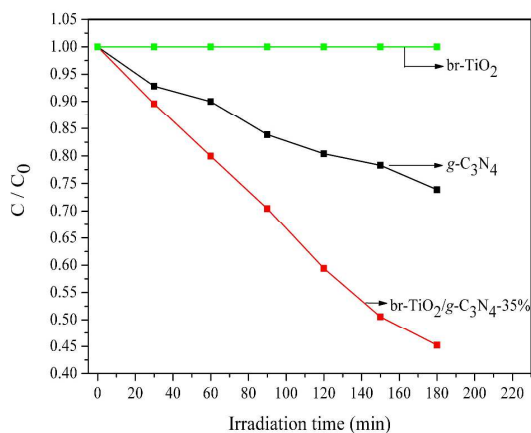


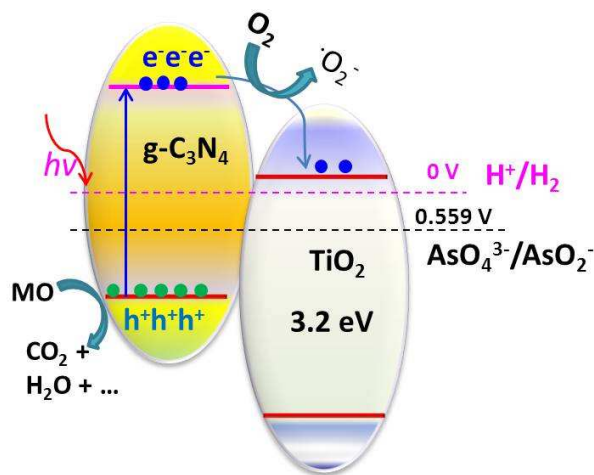
Fig. 7 Oxidation efficiency of As³⁺ by the hybrid br-TiO₂/g-C₃N₄-35%, and components g-C₃N₄ and br-TiO₂ under visible light irradiation.

The hybrid br-TiO₂/g-C₃N₄-35% was successfully applied in MO degradation and hydrogen production. How about its performance in other areas? Herein, we found that the hybrid br-TiO₂/g-C₃N₄-35% had an enhanced activity on As³⁺ oxidation. As indicated in Fig. 7, for our hybrid br-TiO₂/g-C₃N₄-35%, the efficiency for toxic As³⁺ oxidation to form As⁵⁺ reaches as high as 55%. Comparatively, when the irradiation time is set at 3 h, only 26 percent of toxic As³⁺ is oxidized by component g-C₃N₄ as reported elsewhere.³² For another component br-TiO₂, As³⁺ cannot be photo-oxidized at all by visible-light irradiation. Therefore, hybridization of br-TiO₂ improves the oxidation ability of g-C₃N₄.

3.3 Photocatalytic mechanism for hybridization between br-TiO₂ and g-C₃N₄

The above conclusions have proved that when g-C₃N₄ is hybridized with br-TiO₂, photocatalytic activity is improved greatly, relative to g-C₃N₄ or br-TiO₂. It is well known that photocatalytic performance is associated with many factors, such as separation efficiency of the photo-generated electrons and holes, specific surface area, and capacity of the light absorption. g-C₃N₄ is a visible-light-driven photocatalyst with absorption edge at 463 nm (Fig. 4a). The conduction band level of g-C₃N₄ is -1.13 eV and the valence band level is 1.57 eV.¹⁸ Component br-TiO₂ absorbs only ultraviolet light, since the conduction band

level is -0.4 eV and the valence band level is 2.8 eV (all these potential are versus to NHE).^{33,34} The hybrids br-TiO₂/g-C₃N₄ has a response to visible-light as indicated in Fig. 4. When the hybrid br-TiO₂/g-C₃N₄ was irradiated under visible light, the photo-generated electron and hole of g-C₃N₄ was obtained.



Scheme 1 Diagram of band positions and photo-generated electron transferred from component g-C₃N₄ to br-TiO₂ in hybrids br-TiO₂/g-C₃N₄

As shown in Scheme 1, because of the negative conduction band level of g-C₃N₄ relative to br-TiO₂, and because of the existed chemical joint of hybrid br-TiO₂/g-C₃N₄, photo-generated electrons in the conduction band of g-C₃N₄ will migrate to the conduction band of br-TiO₂. The photo-generated electrons and holes could be separated effectively by this process. Furthermore, the valence band levels for both g-C₃N₄ and br-TiO₂ are more positive than E⁰(AsO₄³⁻/AsO₂⁻) = 0.559 eV, while the conduction band level of g-C₃N₄ is more negative than E⁰(H⁺/H₂) = 0 eV, the intimately contacted hybrids br-TiO₂/g-C₃N₄ exhibited a high photocatalytic activity in oxidation of As³⁺ and reduction of water for H₂ evolution.

The separation of the photo-generated carries for the hybrids was characterized by photoluminescence. Fig. 8 gives PL spectra for hybrid br-TiO₂/g-C₃N₄-35%, g-C₃N₄, br-TiO₂ and br-TiO₂/g-C₃N₄-PM. All excitation wavelength of the tests was set at 280 nm. It shows that PL intensity for g-C₃N₄ and br-TiO₂ with main emission peak at 460 and 380 nm, respectively. Both emission peaks for br-TiO₂/g-C₃N₄-35% are greatly decreased in intensity, being weaker than that of br-TiO₂ or g-C₃N₄, and also inferior to br-TiO₂/g-C₃N₄-PM. This result illustrates that the recombination of photo-generated carriers can be effectively restrained through hybridization between br-TiO₂ and g-C₃N₄, as reported in other composite systems.³⁵

For further evidence, the relevant charge transfer process and the recombination rate between the photo-generated carriers were also confirmed by EIS measurements. As displayed in Fig. S6, the curvature of the Nquist circle of br-TiO₂/g-C₃N₄-35% is smaller than that of g-C₃N₄, which reveals that the resistance of br-TiO₂/g-C₃N₄-35% is lower than that of g-C₃N₄. This result illustrates that the hybrid br-TiO₂/g-C₃N₄-35% has a superior separation efficiency of the photo-generated carriers,³⁶ which is beneficial for the enhanced photocatalytic performance.

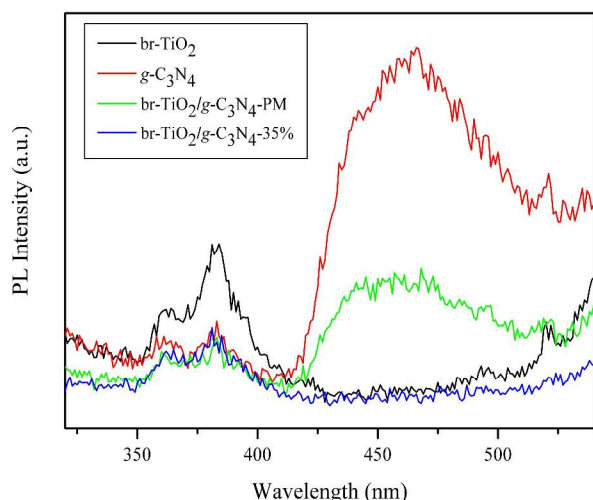


Fig. 8 PL spectra of br-TiO₂/g-C₃N₄-35%, g-C₃N₄, br-TiO₂, and br-TiO₂/g-C₃N₄-PM.

5. Conclusions

Visible-light-driven hybrids br-TiO₂/g-C₃N₄ were synthesized via a simple method for the first time. The physicochemical properties of these hybrids were characterized systematically. We measured and compared the photocatalytic activities of these hybrids to those of the components or the physical mixtures. The br-hybrid TiO₂/g-C₃N₄-35% shows best degradation efficiency in MO degradation. It is worth noting that this hybrid shows an excellent catalytic activity towards As³⁺ oxidation. At the presence of Pt additives, the hybrid is also used for hydrogen production from water splitting. Because of the triple photocatalytic uses, the hybrids reported here are highly promising. Using the current methodology, one may expect more excellent catalysts with multifunction developed for energy and environmental concerns.

20 Acknowledgements

We thank the NSFC (No.91022018, 21025104) and National Basic Research Program of China (No.2011CBA00501, 2013CB933203) for financial support.

Notes and references

- ²⁵ ^a State Key Laboratory of Structural Chemistry, Fujian Institute of Research on the Structure of Matter, Chinese Academy of Sciences, Fuzhou 350002, China. State Key Laboratory of Photocatalysis on Energy and Environment, Fuzhou University, Fuzhou 350002, China. Fax: (+)86-591-83702122; Tel: (+)86-591-83702122; E-mail: guangshe@fjirm.ac.cn
- † Electronic Supplementary Information (ESI) available: [details of any supplementary information available should be included here]. See DOI: 10.1039/b000000x/
- ‡ Footnotes should appear here. These might include comments relevant to but not central to the matter under discussion, limited experimental and spectral data, and crystallographic data.
- Z. D. Meng, L. Zhu, J. G. Choi, M. L. Chen and W. C. Oh, *J. Mater. Chem.*, 2011, **21**, 7596-7603.
 - J. Zhang, Q. L. Xu, S. Z. Qiao and J. G. Yu, *ChemSusChem*, 2013, **6**, 2009-2021.
 - Y.S. Xu, W. D. Zhang, *ChemCatChem*, 2013, **5**(8), 2343-2351.

- B. Mei, A. Pougin and J. Strunk, *J. Catal.*, 2013, **306**, 184-189;
- Y. D. Hou, A. B. Laursen, J. S. Zhang, G. G. Zhang, Y. S. Zhu, X. C. Wang, S. Dahl and I. Chorkendorff, *Angew. Chem. Int. Edit.*, 2013, **52**, 3621-3625.
- Z. Z. Zhang, J. L. Long, L. F. Yang, W. K. Chen, W. X. Dai, X. Z. Fu and X. X. Wang, *Chem. Sci.*, 2011, **2**, 1826-1830.
- A. Dhakshinamoorthy, S. Navalon, A. Corma and H. Garcia, *Energ. Environ. Sci.*, 2012, **5**, 9217-9233.
- X. L. Yang, X. Y. Wang, X. Z. Liu, Y. J. Zhang, W. G. Song, C. Y. Shu, L. Jiang and C. R. Wang, *J. Mater. Chem. A*, 2013, **1**, 8332-8337.
- Y. Tamaki, K. Koike, T. Morimoto, Y. Yamazaki and O. Ishitani, *Inorg. Chem.*, 2013, **52**, 11902-11909.
- B. Zhao, F. Chen, Q. W. Huang and J. L. Zhang, *Chem. Commun.*, 2009, 5115-5117.
- K. Refson, B. Montanari, P. D. Mitev, K. Hermansson and N. M. Harrison, *Phys. Rev. B*, 2013, **88**.
- H. Li, Z. H. Chen, C. K. Tsang, Z. Li, X. Ran, C. Lee, B. Nie, L. X. Zheng, T. F. Hung, J. Lu, B. C. Pan and Y. Y. Li, *J. Mater. Chem. A*, 2014, **2**, 229-236.
- D. O. Scanlon, C. W. Dunnill, J. Buckeridge, S. A. Shevlin, A. J. Logsdail, S. M. Woodley, C. R. A. Catlow, M. J. Powell, R. G. Palgrave, I. P. Parkin, G. W. Watson, T. W. Keal, P. Sherwood, A. Walsh and A. A. Sokol, *Nat. Mater.*, 2013, **12**, 798-801.
- J. T. Park, R. Patel, H. Jeon, D. J. Kim, J. S. Shin and J. H. Kim, *J. Mater. Chem.*, 2012, **22**, 6131-6138.
- J. Y. Liao, B. X. Lei, H. Y. Chen, D. B. Kuang and C. Y. Su, *Energ. Environ. Sci.*, 2012, **5**, 5750-5757.
- G. H. Li and K. A. Gray, *Chem. Mater.*, 2007, **19**, 1143-1146.
- H. F. Lin, L. P. Li, M. L. Zhao, X. S. Huang, X. M. Chen, G. S. Li and R. C. Yu, *J. Am. Chem. Soc.*, 2012, **134**, 8328-8331.
- Y. P. Zang, L. P. Li, Y. Zuo, H. F. Lin, G. S. Li and X. F. Guan, *Rsc Adv.*, 2013, **3**, 13646-13650.
- B. Chai, T. Y. Peng, J. Mao, K. Li and L. Zan, *Phys. Chem. Chem. Phys.*, 2012, **14**, 16745-16752.
- L. Zhang, D. W. Jing, X. L. She, H. W. Liu, D. J. Yang, Y. Lu, J. Li, Z. F. Zheng and L. J. Guo, *J. Mater. Chem. A*, 2014, **2**, 2071-2078.
- K. Sridharan, E. Jang and T. J. Park, *Appl. Catal. B-Environ.*, 2013, **142**, 718-728.
- H. J. Yan and H. X. Yang, *J. Alloy Compd.*, 2011, **509**, L26-L29.
- S. Martha, A. Nashim and K. M. Parida, *J. Mater. Chem. A*, 2013, **1**, 7816-7824.
- S. C. Yan, Z. S. Li and Z. G. Zou, *Langmuir*, 2009, **25**, 10397-10401.
- X. C. Wang, K. Maeda, A. Thomas, K. Takanabe, G. Xin, J. M. Carlsson, K. Domen and M. Antonietti, *Nat. Mater.*, 2009, **8**, 76-80.
- T. Komatsu, *J. Mater. Chem.*, 2001, **11**, 799-801.
- T. Komatsu, *J. Mater. Chem.*, 2001, **11**, 802-805.
- M. L. Zhao, L. P. Li, H. F. Lin, L. S. Yang and G. S. Li, *Chem. Commun.*, 2013, **49**, 7046-7048.
- J. H. Liu, T. K. Zhang, Z. C. Wang, G. Dawson and W. Chen, *J. Mater. Chem.*, 2011, **21**, 14398-14401.
- Y. J. Cui, J. S. Zhang, G. G. Zhang, J. H. Huang, P. Liu, M. Antonietti and X. C. Wang, *J. Mater. Chem.*, 2011, **21**, 13032-13039.
- Y. P. Zang, L. P. Li, X. G. Li, R. Lin and G. S. Li, *Chem. Eng. J.*, 2014, **246**, 277-286.
- J. Hu, S. X. Weng, Z. Y. Zheng, Z. X. Pei, M. L. Huang and P. Liu, *J. Hazard. Mater.*, 2014, **264**, 293-302.
- H. L. Zhao, L. J. Liu, J. M. Andino and Y. Li, *J. Mater. Chem. A*, 2013, **1**, 8209-8216.
- J. G. Yu and J. R. Ran, *Energ. Environ. Sci.*, 2011, **4**, 1364-1371.
- S. X. Weng, B. B. Chen, L. Y. Xie, Z. Y. Zheng and P. Liu, *J. Mater. Chem. A*, 2013, **1**, 3068-3075.
- J. Di, J. X. Xia, S. Yin, H. Xu, M. Q. He, H. M. Li, L. Xu and Y. P. Jiang, *Rsc Adv.*, 2013, **3**, 19624-19631.

A table of contents entry

A visible-light-driven photocatalyst of brookite TiO₂ coupled with g-C₃N₄ exhibited high efficiency for As³⁺ oxidation, MO degradation, hydrogen evolution.

